First publ. in: Journal of Electron Spectroscopy and Related Phenomena ; 184 (2012), 11-12. - pp. 583-588

http://dx.doi.org/10.1016/j.elspec.2011.11.002

Exposure of $[Mn^{III}_6Cr^{III}]^{3+}$ single-molecule magnets to soft X-rays: The effect of the counterions on radiation stability

Andreas Helmstedt[a,*], Marc D. Sacher[a], Aaron Gryzia[a], Alexander Harder[a], Armin Brechling[a], Norbert Müller[a], Ulrich Heinzmann[a], Veronika Hoeke[b], Erich Krickemeyer[b], Thorsten Glaser[b], Samuel Bouvron[c], Mikhail Fonin[c]

[a] *Fakultät für Physik, Universität Bielefeld, Universitätsstraße 25, D-33615 Bielefeld, Germany*
[b] *Fakultät für Chemie, Universität Bielefeld, Universitätsstraße 25, D-33615 Bielefeld, Germany*
[c] *Fachbereich Physik, Universität Konstanz, Universitätsstraße 10, D-78457 Konstanz, Germany*

A B S T R A C T

X-ray absorption spectroscopy studies of the $[Mn^{III}_6Cr^{III}]^{3+}$ single-molecule magnet deposited as a microcrystalline layer on gold substrates are presented. The oxidation state of the manganese centers changes from Mn^{III} to Mn^{II} due to irradiation with soft X-rays. The influence of the charge-neutralizing anions on the stability of $[Mn^{III}_6Cr^{III}]^{3+}$ against soft X-ray exposure is investigated for the different anions tetraphenylborate (BPh_4^-), lactate ($C_3H_5O_3^-$) and perchlorate (ClO_4^-). The exposure dependence of the radiation-induced reduction process is compared for $[Mn^{III}_6Cr^{III}]^{3+}$ with the three different anions.

Keywords:
XAS
Absorption spectroscopy
Reduction
Manganese
Single-molecule magnet
SMM

1. Introduction

With the ongoing development of technology towards smaller devices and structures, more and more efforts are made to assign specific tasks to single molecules. In this context, the so-called single-molecule magnets (SMM) are a promising approach [1]. Single-molecule magnets represent a class of coordination compounds which exhibit a magnetic bistability [2–4]. At low temperatures the existence of an energy barrier for spin reversal leads to a slow relaxation of the magnetization [5,6]. It was recently shown that single-molecule magnets grafted to surfaces do not lose their magnetic properties [7]. This represents an important step towards practical applications of SMM. For Fe_4 complexes [8], a preferential orientation on Au surfaces could be established by chemical means. 3D nanostructures consisting of single-molecule magnets are also being investigated [9].

We have developed the single-molecule magnet $[\{(talen^{t\text{-}Bu_2})Mn^{III}_3\}_2\{Cr^{III}(CN)_6\}]^{3+}$ ($[Mn^{III}_6Cr^{III}]^{3+}$) with $H_6talen^{t\text{-}Bu_2}$ {= 2, 4, 6-tris{1-[2-(3, 5-di-*tert*-butylsalicylaldimino)-2-methylpropylimino]−ethyl}-1, 3, 5-trihydroxybenzene} [10,11]. This molecule contains six Mn^{III} ions arranged in two bowl-shaped trinuclear triplesalen building blocks which are linked by a hexacyanochromate (see Fig. 1). The strongest interaction is the antiferromagnetic coupling of the central Cr^{III} ion with the six terminal Mn^{III} ions, leading to a large spin ground state of $S_t = 21/2$ for the molecule. This high spin ground state in combination with a strong easy-axis magnetic anisotropy and a C_3 symmetry results in an energy barrier for spin-reversal and thus in a slow relaxation of the magnetization at low temperatures. The $[Mn^{III}_6Cr^{III}]^{3+}$ complex can be isolated with different anions which compensate for its triply positive charge. Recently, first results from spin-resolved electron spectroscopy of the manganese centers in $[Mn^{III}_6Cr^{III}]^{3+}$ have been presented and compared to data from reference substances [12]. In the work presented here, the three salts $[Mn^{III}_6Cr^{III}](BPh_4)_3$, $[Mn^{III}_6Cr^{III}](C_3H_5O_3)_3$, and $[Mn^{III}_6Cr^{III}](ClO_4)_3$ using either tetraphenylborate (BPh_4^-), lactate ($C_3H_5O_3^-$) or perchlorate (ClO_4^-) as anions, respectively, were investigated by L-edge X-ray absorption spectroscopy deposited on surfaces.

The investigation of metal-organic compounds containing transition metal centers within an organic ligand structure by

* Corresponding author at: Fakultät für Physik, Universität Bielefeld, Universitätsstraße 25, D-33615 Bielefeld, Germany. Tel.: +49 521 106 5480.
E-mail address: andreas.helmstedt@uni-bielefeld.de (A. Helmstedt).

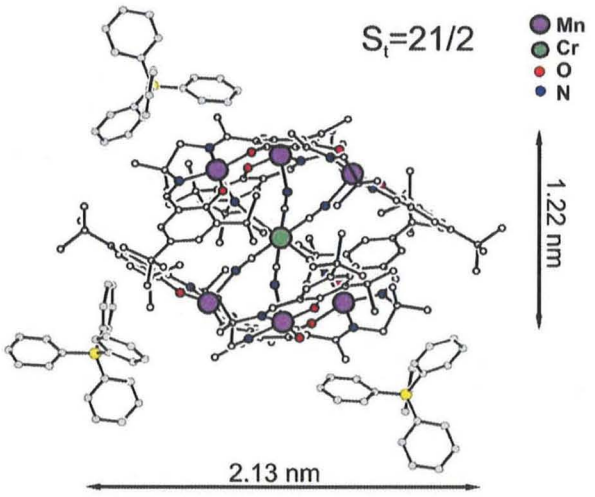

Fig. 1. Molecular structure of $[Mn^{III}_6Cr^{III}]^{3+}$ in crystals of $[Mn^{III}_6Cr^{III}](BPh_4)_3$•4MeCN•2Et$_2$O. The two bowl-shaped triplesalen building blocks each containing three Mn^{III} ions (magenta) are linked by a hexacyanochromate containing a Cr^{III} ion (cyan) [10]. Also shown are the three tetraphenylborate (BPh_4^-) anions.

X-ray-based methods is mostly complicated by the occurrence of radiation damage [13,14]. These damage effects are also well known in protein crystallography [15] using hard X-rays and are possibly caused by the large number of electrons photoexcited in the sample upon irradiation [16]. Radiation damage related to soft X-ray exposure exists also for the $[Mn^{III}_6Cr^{III}]^{3+}$ single-molecular magnets presented here – it is indicated by the reduction of the Mn^{III} metal centers in the SMM to the Mn^{II} oxidation state. The extent of the radiation-induced reduction strongly depends on the choice of anions, which is described in detail below.

2. Sample preparation

$H_6talen^{t\text{-}Bu2}$ {= 2, 4, 6-tris{1-[2-(3, 5-di-*tert*-butylsalicylaldi – mino)-2-methylpropylimino] – ethyl}-1, 3, 5-trihydroxybenzene} and $[\{(talen^{t\text{-}Bu2})Mn^{III}\}_2\{Cr^{III}(CN)_6\}(MeOH)_3(MeCN)_2](BPh_4)_3$• 4MeCN•2Et$_2$O (abbrev. $[Mn^{III}_6Cr^{III}](BPh_4)_3$) were synthesized as described previously [10,17,18]. The perchlorate salt (abbrev. $[Mn^{III}_6Cr^{III}](ClO_4)_3$) was synthesized according to the following procedure described in detail below. $[\{(talen^{t-Bu2})(Mn^{III}(MeOH))_3\}_2\{Cr^{III}(CN)_6\}](ClO_4)_3$. A suspension of $H_6talen^{t\text{-}Bu2}$ (550 mg, 0.495 mmol) and $Mn(OAc)_2$•4H$_2$O (343 mg, 1.40 mmol) in methanol (200 mL) was heated at reflux for 2 h. The resulting brown solution was cooled to room temperature, purged with air for 30 min and heated at reflux for additional 2 h. After cooling to room temperature the reaction solution was treated with a solution of $K_3[Cr(CN)_6]$ (81 mg, 0.25 mmol) in water (5 mL). The reaction mixture was stirred at room temperature for 60 min and filtered. A solution of $NaClO_4$•H$_2$O (1645 mg, 11.71 mmol) in methanol (40 mL) was added to the filtrate. The reaction mixture was stirred at room temperature for 10 min and filtered again. Stirring of the filtrate for 16 h at room temperature resulted in the formation of a brown precipitate, which was collected by filtration and dried in vacuo. The resulting brown powder was dissolved in methanol. Slow diffusion of diethyl ether into the solution afforded large black crystals. Yield: 223 mg (28%). ESI-MS (MeCN): *m/z*: 915.9 $[\{(talen^{t\text{-}Bu2})Mn_3\}_2\{Cr(CN)_6\}]^{3+}$, 1374.2 $[\{(talen^{t\text{-}Bu2})Mn_3\}_2\{Cr(CN)_6\}]^{2+}$, 2747.2 $[\{(talen^{t\text{-}Bu2})Mn_3\}_2\{Cr(CN)_6\}]^{+}$; MALDI-TOF-MS (matrix DCTB): *m/z*: 2946.5 $\{[\{(talen^{t\text{-}Bu2})Mn_3\}_2\{Cr(CN)_6\}](ClO_4)_2\}^{+}$, 2846.9 $\{[\{(talen^{t\text{-}Bu2})Mn_3\}_2\{Cr(CN)_6\}]ClO_4\}^{+}$, 2746.4 $[\{(talen^{t\text{-}Bu2})Mn_3\}_2\{Cr(CN)_6\}]^{+}$; IR (KBr): $\tilde{\nu}$ (cm^{-1}) = 2957m, 2907m, 2870m, 2156w, 1613s, 1567s, 1539s, 1493vs, 1437m, 1395m, 1363m, 1339m, 1310m, 1275s, 1254s, 1188m, 1153m, 1142m, 1121m, 1090m, 1063m, 1026w, 845m, 820w, 779w, 750w, 642w, 625w, 608w, 575m, 552m. Elemental analysis (%): calcd for $C_{150}H_{216}N_{18}O_{30}Cl_3CrMn_6$: C 55.62, H 6.72, N 7.78; found: C 55.49, H 6.64, N 7.87.

$[\{(talen^{t-Bu2})(Mn^{III}(MeOH))_3\}_2\{Cr^{III}(CN)_6\}](C_3H_5O_3)_3$•9MeOH was prepared similarly using D,L-$C_3H_5O_3Na$ instead of $NaClO_4$•H$_2$O. The resulting substance is abbreviated as $[Mn^{III}_6Cr^{III}](C_3H_5O_3)_3$ in this publication. Further details will be published in a forthcoming article.

Crystalline batches of the $[Mn^{III}_6Cr^{III}]^{3+}$ salts were checked by X-ray diffraction (XRD) and infrared spectroscopy (see above) with regard to their desired chemical and physical properties. Solutions of the $[Mn^{III}_6Cr^{III}]^{3+}$ salts with a concentration of 4.5×10^{-4} mol/l were prepared by dissolving the compounds in methanol.

For the measurements presented here, 10 μl of the methanolic solutions of $[Mn^{III}_6Cr^{III}](BPh_4)_3$ and $[Mn^{III}_6Cr^{III}](ClO_4)_3$ were dripped on horizontally oriented square substrates with an edge length of 5.5 ± 1.0 mm. For $[Mn^{III}_6Cr^{III}](ClO_4)_3$ microcrystallites began to grow in the liquid phase during solvent evaporation and to form a granular deposit on the substrate surface. The particle heights vary between 250 nm and 3000 nm, a large fraction of the microcrystallites show a height of 500 ± 250 nm (see Fig. 2). The area coverage is about 30%.

By optical microscopy the $[Mn^{III}_6Cr^{III}](BPh_4)_3$ sample reveals a closed deposit layer with only small, irregular aggregations of microcrystallites on top. The abundance of microcrystallites is much lower than for $[Mn^{III}_6Cr^{III}](ClO_4)_3$ and increases towards the sample edges. Particle sizes are comparable to those found for the SMM samples with perchlorate anions.

The methanolic solution of $[Mn^{III}_6Cr^{III}](C_3H_5O_3)_3$ shows a completely different wetting behaviour: No optically discernible crystallites form in this case, but a plain deposit layer without recognizable structures instead. Only 5 μl of this solution was necessary to form a complete layer.

All SMM samples prepared as described reveal a border area consisting of macroscopic deposits near the substrate edges. The substrates used for our investigations are commercially available[1]

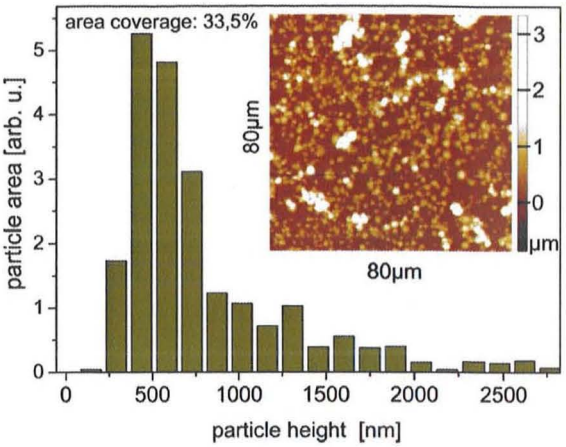

Fig. 2. Particle height distribution in a 80 μm by 80 μm area of a $[Mn^{III}_6Cr^{III}](ClO_4)_3$ microcrystallite sample, derived from the AFM scan shown in the inset.

[1] Brand name: Arrandee, Manufacturer: Dr. Dirk Schröer, Schlossstrasse 94, D-33824 Werther, Germany.

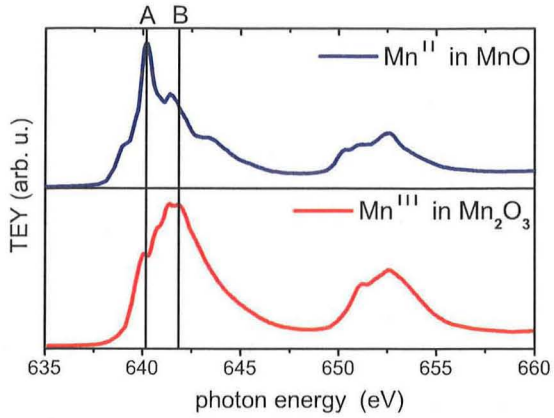

Fig. 3. Manganese $L_{2,3}$-edge XAS spectra obtained from bulk manganese oxides MnO and Mn_2O_3. The markings **A** and **B** indicate Mn^{II} (**A**) and Mn^{III} (**B**) specific absorption features.

and consist of a borosilicate glass plate coated with 2.5 ± 1.5 nm Cr and 250 ± 50 nm Au on top. For comparison, samples have also been prepared on silicon and HOPG substrates of comparable size.

3. Experimental details

Infrared spectra (400–4000 cm^{-1}) of solid samples were recorded on a Shimadzu FT-IR 8400S as KBr disks. ESI and MALDI-TOF mass spectra were recorded on a Bruker Esquire 3000 ion trap mass spectrometer and a PE Biosystems Voyager DE mass spectrometer, respectively. Elemental analyses were carried out on a LECO CHN-932 or a HEKAtech Euro EA elemental analyzer.

The oxidation states of the manganese centers were probed by X-ray absorption spectroscopy (XAS) at the Mn-$L_{2,3}$ edge. These measurements were performed in total electron yield mode by measuring the sample current. The substrate surface was electrically connected to the sample holder by conductive adhesive tape. Besides the reference data in Fig. 3 (measured at beamline UE52-SGM, BESSY II), the measurements presented here were carried out at beamline D1011 of MAX-lab in Lund. This bending-magnet beamline delivers a photon flux of about 10^{10} photons/s into a spot size of 1 mm^2 in the relevant energy range of 600–700 eV. The comparatively low flux reduces the speed of the radiation-induced changes of the sample properties. Given a monochromator exit slit width of 6 μm, the energy resolution is about 120 meV in the energy range used. All measurements were performed at room temperature. In the case of Mn_{12} single-molecule magnets, no temperature dependence of the reduction process was found before [19]. For a di(μ-oxo)$Mn^{III}Mn^{IV}$ complex, photoreduction by X-ray exposure was detected even at temperatures as low as 20 K [20]. However, L-edge XAS investigations of Co- and Fe-containing complexes exhibit a significantly slower photoreduction at 50 K compared to 298 K [21], so a possible temperature dependence cannot be excluded for $\mathbf{[Mn^{III}_6Cr^{III}]^{3+}}$. The oxidation state of the manganese centers during X-ray exposure was monitored by sequences of 20–26 consecutive XAS scans at the identical irradiated sample area. This ensures that the investigation of the radiation-induced changes of the sample is not influenced by varying amounts of material on different sample positions. If the occurring change was sufficiently small, the photon flux was increased by changing the width of the monochromator exit slit. A single XAS scan needed about 4–5 min.

Due to the presence of a chromium background signal caused by Cr used in the coating of beamline optical elements [22], high-sensitivity measurements at the Cr $L_{2,3}$-edge were strongly impaired. Therefore no XAS measurements of the central Cr^{III} ion are presented here.

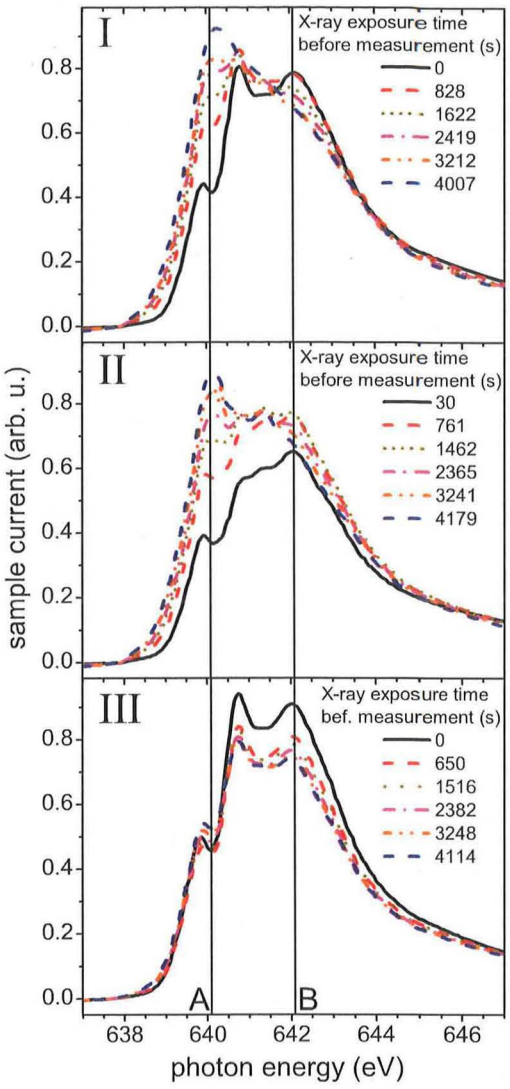

Fig. 4. Selected scans from three series of consecutively recorded XAS spectra of $\mathbf{[Mn^{III}_6Cr^{III}]^{3+}}$ with the different anions tetraphenylborate (**I**), lactate (**II**) and perchlorate (**III**). The radiation-induced change in the sample condition is indicated by the change in X-ray absorption at photon energies **A** and **B**. For a quantitative analysis of the complete series see Fig. 5.

All XAS spectra have been adjusted to zero in the pre-edge and normalized to 1 in the post-edge region of the Mn-$L_{2,3}$ absorption. Differences in the energy calibration of synchrotron beamlines result in shifts in the energy scale – all results shown in this work were corrected to match the reference data in Fig. 3. These data have been recorded following a monochromator calibration.

4. Results and discussion

4.1. Radiation-induced reduction process

The $L_{2,3}$ edge XAS spectra of MnO and Mn_2O_3 shown in Fig. 3 serve as references. The X-ray absorption spectra of $\mathbf{[Mn^{III}_6Cr^{III}]^{3+}}$ samples without preexposure show a typical multiplet structure in the Mn-L_3-edge region (see Fig. 4). The broad absorption maximum at 642 eV marked **B** is a characteristic absorption feature of manganese in the Mn^{III} oxidation state [23] (see Fig. 3). A small

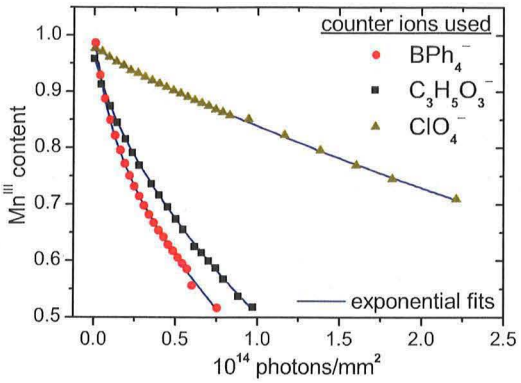

Fig. 5. Relation between accumulated X-ray exposure and Mn^{III} content for $[Mn^{III}_6Cr^{III}]^{3+}$ with the different anions lactate ($C_3H_5O_3^-$), tetraphenylborate (BPh_4^-) or perchlorate (ClO_4^-). The conversion from exposure time to photon number is explained in the text.

shoulder, also originating from Mn^{III}, exists at about 640 eV in the rising edge of the main peak. This spectral shape of the manganese-L_3 absorption peak indicates the presence of Mn^{III} not only in bulk oxides, but also in a molecular environment [19,24,25].

Being exposed to soft X-rays, $[Mn^{III}_6Cr^{III}]^{3+}$ samples reveal characteristic changes in the shape of the manganese L_3 absorption spectrum. With increasing radiation dose the change of the sample condition is visible as a continuous increase of absorption at the photon energy marked **A** – a large peak which coincides with the MnO absorption maximum [24] (see Fig. 3) develops at 640.1 eV and indicates the presence of a growing fraction of Mn^{II}. Simultaneously the absorption in the Mn^{III} maximum marked **B** continuously decreases. This process is visualized for $[Mn^{III}_6Cr^{III}]^{3+}$ single molecule magnets with the different anions by series of consecutive XAS scans covering a total exposure time of about 4000 s (Fig. 4).

With the absorption peaks **A** and **B** being characteristic for the oxidation states Mn^{II} and Mn^{III} of the SMM manganese centers, respectively, the ratio **B/A** can be used as an indicator for the oxidation state of the Mn constituents in the investigated SMM samples. The intact molecule contains only manganese in the Mn^{III} state [10], so the increasing Mn^{II} absorption indicates a progressive reduction of Mn^{III} to Mn^{II} due to X-ray exposure.

The synchrotron radiation intensity reaching the sample is not necessarily constant during a series of measurements: It depends on the (slowly decreasing) storage ring current as well as on technical parameters like the selected monochromator exit slit width. It is therefore necessary to convert exposure times into numbers of photons reaching the sample by using the beamline-specific relation between photon energy, ring current and available photon flux, usually provided in the beamline datasheet. The photon numbers given in Fig. 5 represent the total exposure up to the time when the Mn-L_3 peak is reached in the respective XAS scan. This means that not only the radiation exposure from previous measurements is taken into account, but also the radiation dose hitting the sample in the current run until the Mn-L_3 peak region is reached. As both oxidation states Mn^{II} and Mn^{III} contribute to the absorption at photon energies **A** and **B** (see Fig. 3), the **B/A** peak ratio does not directly represent the ratio of Mn^{III} to Mn^{II} present in the sample. Based on Mn^{II} and Mn^{III} reference data obtained from $Mn^{II}O$ and $Mn^{III}{}_2O_3$ the following estimation was performed: Mn^{III} and Mn^{II} reference spectra each were normalized for their L_3 photoionization cross sections. Then both reference spectra were added up with the Mn^{III} fraction varied from $Mn^{III}/(Mn^{III}+Mn^{II})=1$ to zero. For the resulting sum spectra, the **B/A** peak ratio was determined as a function of the Mn^{III} fraction. The functional dependence $Mn^{III}/(Mn^{III}+Mn^{II})=f(B/A)$ derived from these data was used to determine the Mn^{III} content in the SMM samples from the measured **B/A** peak ratio. The results are presented in Fig. 5.

The three $[Mn^{III}_6Cr^{III}]^{3+}$ salts show a different radiation sensitivity: While the radiation-induced reduction of Mn^{III} to Mn^{II} and therewith the decrease of the Mn^{III} content of $[Mn^{III}_6Cr^{III}](C_3H_5O_3)_3$ differs only slightly from the data obtained for $[Mn^{III}_6Cr^{III}](BPh_4)_3$, the reduction process is remarkably slower for $[Mn^{III}_6Cr^{III}](ClO_4)_3$. A Mn^{III} fraction of 0.75 is reached for $[Mn^{III}_6Cr^{III}](BPh_4)_3$ and $[Mn^{III}_6Cr^{III}](C_3H_5O_3)_3$ after a radiation dose of 2.2×10^{13} and 3.2×10^{13} photons/mm^2, respectively. An identical degree of sample reduction is found for $[Mn^{III}_6Cr^{III}](ClO_4)_3$ not until an X-ray exposure of 1.8×10^{14} photons/mm^2 has been accumulated. Compared to the average photon dose of approx. 3×10^{12} photons/mm^2 needed for a single XAS scan, this allows the acquisition of 7 (10) absorption spectra for the case of tetraphenylborate (lactate) anions. Using perchlorate anions the same degree of sample reduction will occur after approx. 60 XAS acquisitions.

The differences in the radiation sensitivity of the $[Mn^{III}_6Cr^{III}]^{3+}$ salts correlate with the redox properties of the anions. In contrast to perchlorate, which is a strong oxidant [26], tetraphenylborate [27] and lactate [28] are reducing agents which may easily release electrons upon irradiation and thus mediate the conversion of Mn^{III} to Mn^{II}. In protein crystallography [13,15] it was shown that radiation-induced reduction of metal centers in proteins can be attributed to the large number of electrons released either directly upon photon absorption or by secondary processes like thermalization of high energy photo- or Auger electrons [16]. Photoreduction processes also occur when X-ray-based methods are applied to single-molecule magnets: For the well known Mn_{12} molecules [29], a radiation-induced reduction of Mn in the Mn^{IV} and Mn^{III} oxidation states to Mn^{III} and Mn^{II}, respectively, has been detected [19]. Apart from Mn_{12}, other SMM species as the 'ferric wheel' $NaFe_6$ [30], the 'ferric star' Fe_4 [31] and the 'manganese wheel' Mn_7 [32] also show X-ray-induced radiation damage: The metal ions responsible for the magnetic properties of the SMM molecules are reduced [33]. The decrease of the Mn^{III} content with soft X-ray exposure observed on the $[Mn^{III}_6Cr^{III}]^{3+}$ samples agrees with a fit function representing the sum of two exponential decays (solid lines in Fig. 5) with two different decay constants t_1, t_2 with $t_1<t_2$. While t_1 influences the decay for low photon exposure, the slower decay with t_2 predominates for larger radiation doses. The fit function and the full set of fit parameters are given in Table 1.

Table 1
Fit function and resulting fit parameters for the radiation-induced Mn^{III} to Mn^{II} reduction process shown in Fig. 5.

Fit function: $y=A_1\times\exp(-x/t_1)+A_2\times\exp(-x/t_2)$								
Anion	Fit parameter							
	A_1	ΔA_1	$t_1/10^{13}$	$\Delta t_1/10^{13}$	A_2	ΔA_2	$t_2/10^{13}$	$\Delta t_2/10^{13}$
BPh_4^-	0.13	0.01	1.02	0.10	0.85	0.01	15.0	0.44
$C_3H_5O_3^-$	0.06	0.005	1.15	0.17	0.90	0.005	17.4	0.24
ClO_4^-	0.01	0.002	1.74	0.53	0.96	0.002	71.4	0.71

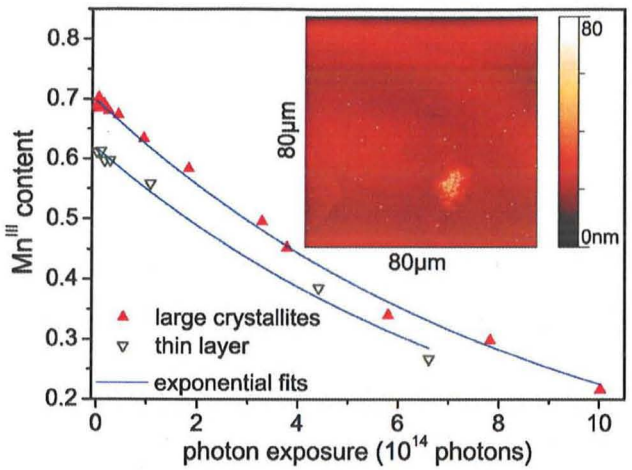

Fig. 6. Relation between accumulated X-ray exposure and Mn^{III} content for $[Mn^{III}_6Cr^{III}](ClO_4)_3$ and two different deposit morphologies. The solid lines represent exponential fits to the data, the resulting decay constants are given in the text. Inset: AFM micrograph of the sample with the thin deposit layer. See Fig. 2 for comparison.

4.2. Sample morphology

The $[Mn^{III}_6Cr^{III}]^{3+}$ salts with different anions show significantly different deposition behaviours on the substrate surface, therefore a possible influence of the sample morphology on the investigated stability against X-ray exposure has to be considered. The highest stability was found for the SMM compound using perchlorate anions, which forms a dense layer of large crystallites on the gold substrate (see Fig. 2). Besides the preparation process mentioned before, a diluted solution of $[Mn^{III}_6Cr^{III}](ClO_4)_3$ with a 5 times lower concentration (approx. 9×10^{-5} mol/l) was used to prepare another set of two samples of this compound for comparison. Due to the lower concentration of SMM in this case, a plain deposit layer with only a few scattered microcrystallites is formed upon solvent evaporation (see Fig. 6, inset), resembling closely the deposition behaviour of the SMM using tetraphenylborate anions. The sample prepared with the concentration of 4.5×10^{-4} mol/l as before showed a deposit layer comparable to that in Fig. 2 as expected. Nevertheless, an evaluation of the radiation-induced reduction process for the two different deposit morphologies (see Fig. 6) shows comparable decay constants of $(89 \pm 2) \times 10^{13}$ (thin layer) and $(86 \pm 4) \times 10^{13}$ (large crystallites). Compared to the effect of the different choice of anions, no significant influence of the sample morphology on the radiation stability has been observed here.

Regarding the data in Fig. 6, it is striking that both curves show a significantly reduced Mn^{III} content at zero radiation exposure. A detailed investigation of this finding in a recent beamtime lead to the observation of a sample deterioration caused by the Bayert-Alpert (BA) ionization gauge in the loadlock of the apparatus. Storage of the samples in the neighbourhood of the BA gauge operating at pressures of 10^{-5} to 10^{-6} mbar for usual pump-down times of 20 min to 1 h lead to a considerable reduction effect (see Fig. 7) comparable to the radiation damage shown in Fig. 4. The detrimental effects of ionization gauge operation depend on the vacuum conditions: No discernible reduction effect was found for samples stored in the preparation chamber for several days while operating an ionization gauge at a pressure of approx. 10^{-10} mbar.

4.3. Substrate influence

In order to identify a possible influence of the substrate material on the sample reduction, the XAS scan series were repeated

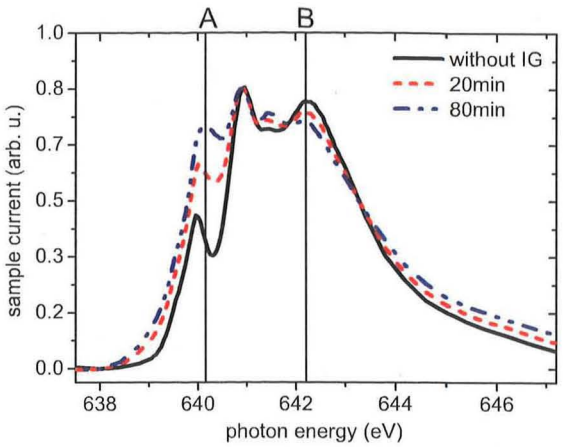

Fig. 7. Deterioration of $[Mn^{III}_6Cr^{III}]^{3+}$ samples due to ionization gauge operation at pressures of 10^{-5} to 10^{-6} mbar. A reduction effect comparable to the radiation damage is visible by the change in the **B/A** absorption peak ratio.

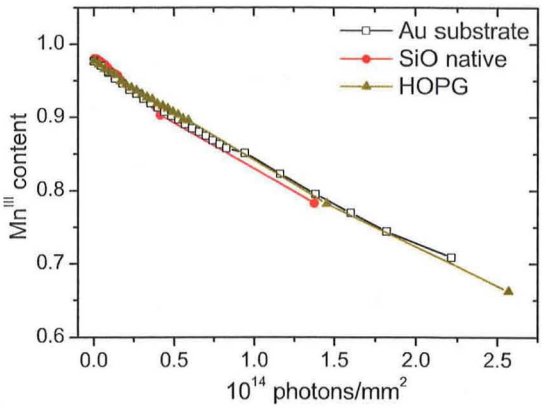

Fig. 8. Comparison of the radiation-induced SMM reduction process for different substrate materials. The measurements were performed on $[Mn^{III}_6Cr^{III}](ClO_4)_3$.

for $[Mn^{III}_6Cr^{III}](ClO_4)_3$ on different substrates. Besides the gold substrates already mentioned, HOPG and silicon with a native oxide layer of about 2 nm were used.

For the investigated substrate materials and the applied radiation doses, no significant influence of the choice of substrate on the radiation-induced SMM reduction process could be observed (see Fig. 8). While this has been experimentally shown for different microcrystallite layers (see Figs. 2 and 6), the situation might be expected to be different for very thin adsorbate layers down to monolayer thickness: For Mn_{12} single-molecule magnets the molecule-substrate-interaction in the monolayer and submonolayer regime leads to a reduction of the metal ions in the SMM upon adsorption [34]. Detailed XAS studies of Mn_{12} layers deposited by an electrospray process with resulting layer thicknesses ranging from 0.2 ML to 2.5 ML [35] confirm the systematic reduction of adsorbed Mn_{12} and attribute the effect to charge transfer interactions with the substrate.

5. Conclusions

The exposure of $[Mn^{III}_6Cr^{III}]^{3+}$ single-molecule magnets to soft X-rays leads to a radiation-induced reduction process. This is indicated by a change in the oxidation state of the SMM manganese centers from Mn^{III} to Mn^{II}, which can be deduced from characteristic changes in the X-ray absorption at the manganese L_3-edge.

The velocity of the reduction process and consequently the radiation sensitivity of the $[Mn^{III}_6Cr^{III}]^{3+}$ molecule strongly depends on the choice of anions. No dependence on the morphology of the SMM adsorbate layer was observed. In the case of perchlorate (ClO_4^-) anions instead of tetraphenylborate (BPh_4^-) or lactate ($C_3H_5O_3^-$), a comparable degree of sample reduction requires a radiation dose eight times higher.

A substrate influence on the radiation-induced reduction of $[Mn^{III}_6Cr^{III}]^{3+}$ could not be detected on the microcrystalline samples investigated in this work. This might be expected to be different for very thin adsorbate layers down to monolayer thickness due to the increasing molecule-substrate interaction.

Acknowledgements

Special thanks are due to MAX-lab, Lund, HZB Berlin (BESSY II) and their staff for continuous support at the beamlines. This work is supported by the Deutsche Forschungsgemeinschaft within Research Unit 945 and Collaborative Research Center 767. M. F. and S. B. acknowledge financial support from the Baden-Württemberg Stiftung.

References

[1] L. Bogani, W. Wernsdorfer, Nat. Mater. 7 (2008) 179–186.
[2] R. Sessoli, D. Gatteschi, A. Caneschi, M.A. Novak, Nature 365 (1993) 141–143.
[3] R. Sessoli, H.L. Tsai, A.R. Schake, S.Y. Wang, J.B. Vincent, K. Folting, D. Gatteschi, G. Christou, D.N. Hendrickson, J. Am. Chem. Soc. 115 (1993) 1804–1816.
[4] G. Christou, D. Gatteschi, D.N. Hendrickson, R. Sessoli, MRS Bull. 25 (2000) 66–71.
[5] D. Gatteschi, R. Sessoli, Angew. Chem. Int. Ed. 42 (2003) 268–297.
[6] D. Gatteschi, R. Sessoli, J. Villain, Molecular Nanomagnets, Oxford University Press, Oxford, 2006.
[7] M. Mannini, F. Pineider, P. Sainctavit, C. Danieli, E. Otero, C. Sciancalepore, A.M. Talarico, M.-A. Arrio, A. Cornia, D. Gatteschi, R. Sessoli, Nat. Mater. 8 (2009) 194–197.
[8] M. Mannini, F. Pineider, C. Danieli, F. Totti, L. Sorace, Ph Sainctavit, M.-A. Arrio, E. Otero, L. Joly, J.C. Cezar, A. Cornia, R. Sessoli, Nature 468 (2010) 417–421.
[9] G. Rogez, B. Donnio, E. Terazzi, J.-L. Gallani, J.-P. Kappler, J.-P. Bucher, M. Drillon, Adv. Mater. 21 (2009) 4323–4333.
[10] T. Glaser, M. Heidemeier, T. Weyhermüller, R.-D. Hoffmann, H. Rupp, P. Müller, Angew. Chem. Int. Ed. 45 (2006) 6033–6037.
[11] T. Glaser, Chem. Commun. 47 (2011) 116–130.
[12] A. Helmstedt, N. Müller, A. Gryzia, N. Dohmeier, A. Brechling, M.D. Sacher, U. Heinzmann, V. Hoeke, E. Krickemeyer, T. Glaser, S. Bouvron, M. Fonin, M. Neumann, J. Phys.: Condens. Matter 23 (2011) 266001.
[13] J. Yano, J. Kern, K.-D. Irrgang, M.J. Latimer, U. Bergmann, P. Glatzel, Y. Pushkar, J. Biesiadka, B. Loll, K. Sauer, J. Messinger, A. Zouni, V.K. Yachandra, PNAS 102 (2005) 12047–12052.
[14] L. Rulíšek, U. Ryde, J. Phys. Chem. B 110 (2006) 11511–11518.
[15] M. Grabolle, M. Haumann, C. Müller, P. Liebisch, H. Dau, J. Biol. Chem. 281 (2006) 4580–4588.
[16] C.M. Wilmot, T. Sjögren, G.H. Carlsson, G.I. Berglund, J. Hajdu, Methods Enzymol. 353 (2002) 301–318.
[17] T. Glaser, M. Heidemeier, T. Lügger, Dalton Trans. (2003) 2381–2383.
[18] T. Glaser, M. Heidemeier, R. Fröhlich, P. Hildebrandt, E. Bothe, E. Bill, Inorg. Chem. 44 (2005) 5467–5482.
[19] S. Voss, M. Fonin, L. Burova, M. Burgert, Y.S. Dedkov, A.B. Preobrajenski, E. Goering, U. Groth, A.R. Kaul, U. Ruediger, Appl. Phys. A 94 (2009) 491–495.
[20] L. Dubois, L. Jacquamet, J. Pécaut, J.-M. Latour, Chem. Commun. (2006) 4521–4523.
[21] D. Collison, C.D. Garner, C.M. McGrath, J.F.W. Mosselmans, M.D. Roper, J.M.W. Seddon, E. Sinn, N.A. Young, J. Synchr. Rad. 6 (1999) 585–587.
[22] J. Schnadt, J. Schiessling, J.N. O'Shea, L. Patthey, M. Shi, C. Puglia, N. Mårtensson, P.A. Brühwiler, Nucl. Instrum. Methods B 184 (2001) 609–614.
[23] S.P. Cramer, F.M.F. deGroot, Y. Ma, C.T. Chen, F. Sette, C.A. Kipke, D.M. Eichhorn, M.K. Chan, W.H. Armstrong, E. Libby, G. Christou, S. Brooker, V. McKee, O.C. Mullins, J.C. Fuggleg, J. Am. Chem. Soc. 113 (1991) 7937–7940.
[24] M. Prinz, M. Raekers, M. Neumann, K. Kuepper, S. Khanra, T. Weyhermüller, P. Chaudhuri, Z. Phys. Chem. 223 (2009) 145–155.
[25] M.M. Grush, Y. Muramatsu, J.H. Underwood, E.M. Gullikson, D.L. Ederer, R.C.C. Perera, T.A. Callcott, J. Electron Spectrosc. Relat. Phenom. 92 (1998) 225–229.
[26] A.F. Hollemann, E. Wiberg, N. Wiberg, Lehrbuch der Anorganischen Chemie, deGruyter, Berlin, 2007.
[27] P.K. Pal, S. Chowdhury, M.G.B. Drew, D. Datta, New J. Chem. 26 (2002) 367–371.
[28] T. Bücher, M. Klingenberg, Angew. Chem. 70 (1958) 552–570.
[29] R.W. Saalfrank, T. Nakajima, N. Mooren, A. Scheurer, H. Maid, F. Hampel, C. Trieflinger, J. Daub, Eur. J. Inorg. Chem. (2005) 1149–1153.
[30] R.W. Saalfrank, I. Bernt, E. Uller, F. Hampel, Angew. Chem. Int. Ed. Engl. 36 (1997) 2482–2485.
[31] R.W. Saalfrank, I. Bernt, M.M. Chowdhry, F. Hampel, G.B.M. Vaughan, Chem. Eur. J. 7 (2001) 2765–2769.
[32] R.W. Saalfrank, A. Scheurer, R. Prakash, F.W. Heinemann, T. Nakajima, F. Hampel, R. Leppin, B. Pilawa, H. Rupp, P. Müller, Inorg. Chem. 46 (2007) 1586–1592.
[33] N. Schmidt, A. Scheurer, S. Sperner, R.H. Fink, Z. Naturforsch. 65b (2010) 390–398.
[34] M. Mannini, P. Sainctavit, R. Sessoli, C. Cartier dit Moulin, F. Pineider, M.-A. Arrio, A. Cornia, D. Gatteschi, Chem. Eur. J. 14 (2008) 7530–7535.
[35] A. Saywell, A.J. Britton, N. Taleb, M. del Carmen Giménez-López, N.R. Champness, P.H. Beton, J.N. O'Shea, Nanotechnology 22 (2011) 075704.